Supporting Information for: "Electrostatics, Charge Transfer, and the Nature of the Halide–Water Hydrogen Bond"

John M. Herbert*and Kevin Carter-Fenk
Department of Chemistry & Biochemistry, The Ohio State University

January 21, 2021

*herbert@chemistry.ohio-state.edu

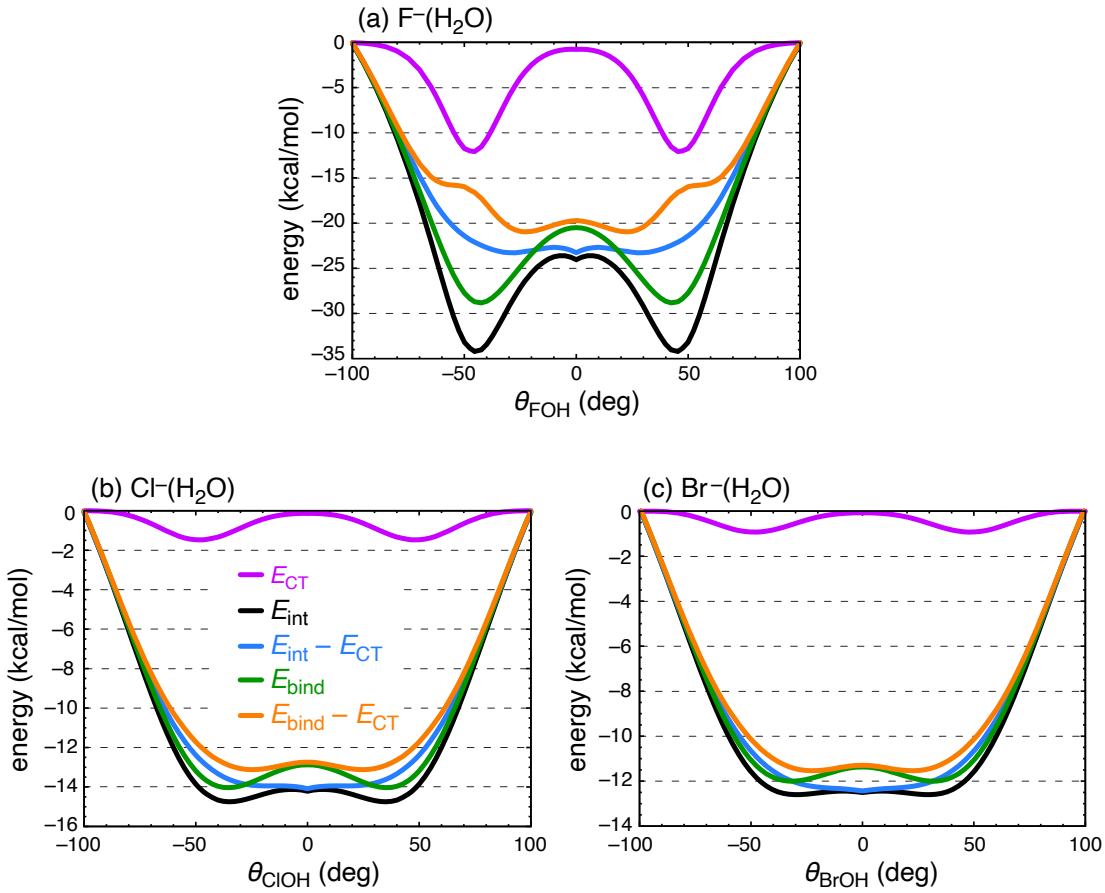

Figure S1: Relaxed scans along the angle θ_{XOH} for (a) $F^-(H_2O)$, (b) $Cl^-(H_2O)$, and (c) $Br^-(H_2O)$. Interaction energies (E_{int}) are obtained from SAPT0 + δE_{HF}/jun-cc-pVDZ calculations and H_2O relaxation energies (E_{rlx}) are computed at the CCSD(T)/aug-cc-pVQZ level. These energies are then combined to obtain $E_{\mathrm{bind}} = E_{\mathrm{int}} + E_{\mathrm{rlx}}$. For each system, the minimum of $E_{\mathrm{int}} - E_{\mathrm{CT}}$ lies at the C_{2v} geometry, providing an unambiguous demonstration that CT drives the preference for hydrogen bonding. The $E_{\mathrm{bind}} - E_{\mathrm{CT}}$ curves exhibit shallow minima away from the C_{2v} geometry but at angles θ_{XOH} that are quite compressed compared to normal, quasi-linear hydrogen bonds. The E_{int} and $E_{\mathrm{int}} - E_{\mathrm{CT}}$ data here are the same as those plotted in Fig. 6.

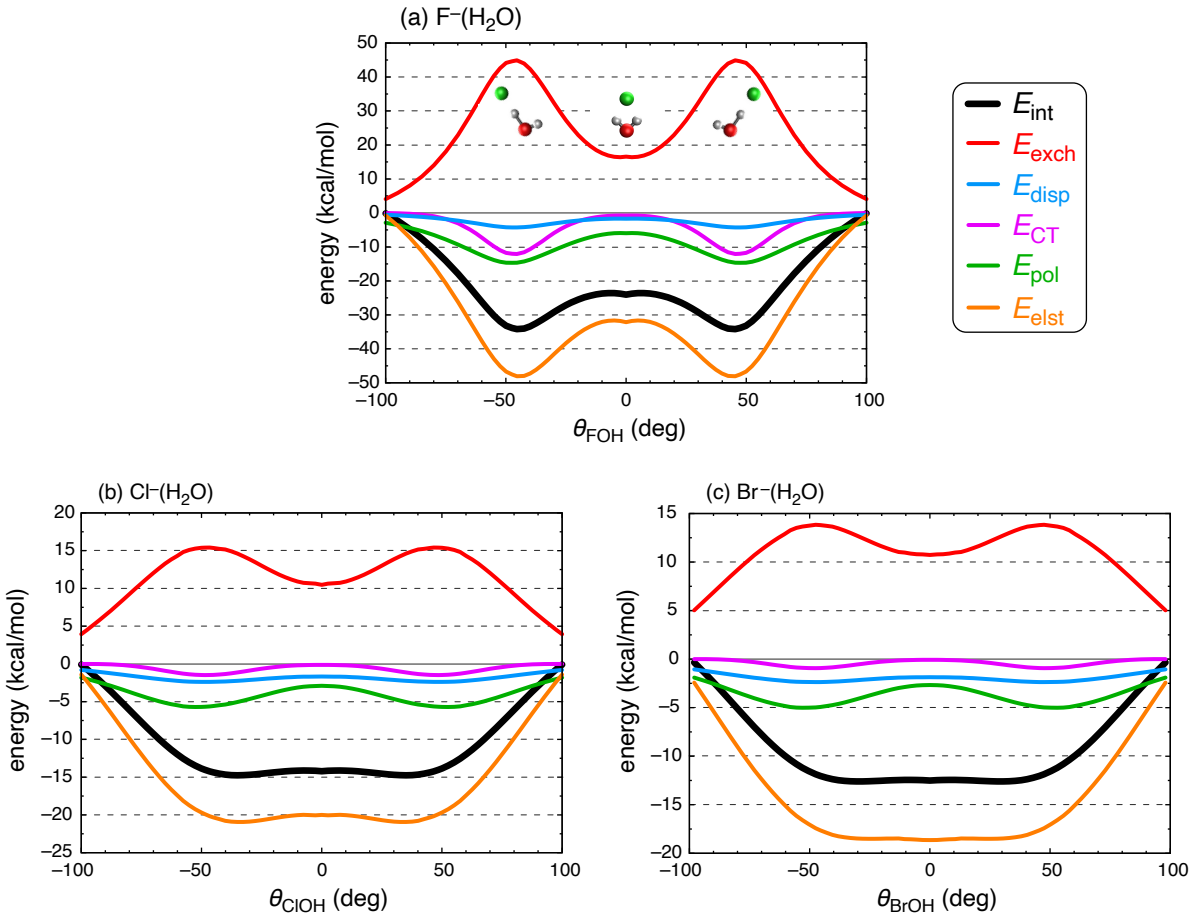

Figure S2: Relaxed scans of θ_{XOH} for (a) $F^-(H_2O)$, (b) $Cl^-(H_2O)$, and (c) $Br^-(H_2O)$, illustrating energy components computed at the SAPT0 + δE_{HF}/jun-cc-pVDZ level. Ball-and-stick models in (a) show the asymmetry of the O–H bond lengths that emerges in the hydrogen-bonded minima. The sum of the five components equals the total interaction energy, E_{int}. Panel (a) is the same as Fig. 4.

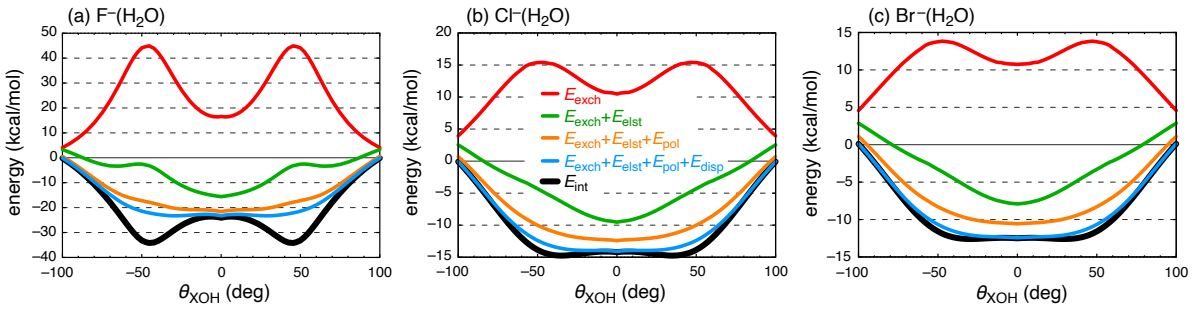

Figure S3: Relaxed scans along θ_{XOH} for (a) $F^-(H_2O)$, (b) $Cl^-(H_2O)$, and (c) $Br^-(H_2O)$, illustrating sequential construction of the SAPT0 + δE_{HF} interaction potential, $E_{\mathrm{int}}(\theta_{\mathrm{XOH}})$. In each panel, the full interaction potential (E_{int}) is assembled term-by-term, as indicated by the common legend that is shown in (b). The CT energy is not included here but can be surmised from the difference between E_{int} and $E_{\mathrm{exch}} + E_{\mathrm{elst}} + E_{\mathrm{disp}} + E_{\mathrm{pol}}$. As compared to the analogous plots in Fig. 5, these plots add together the energy components in a different order.

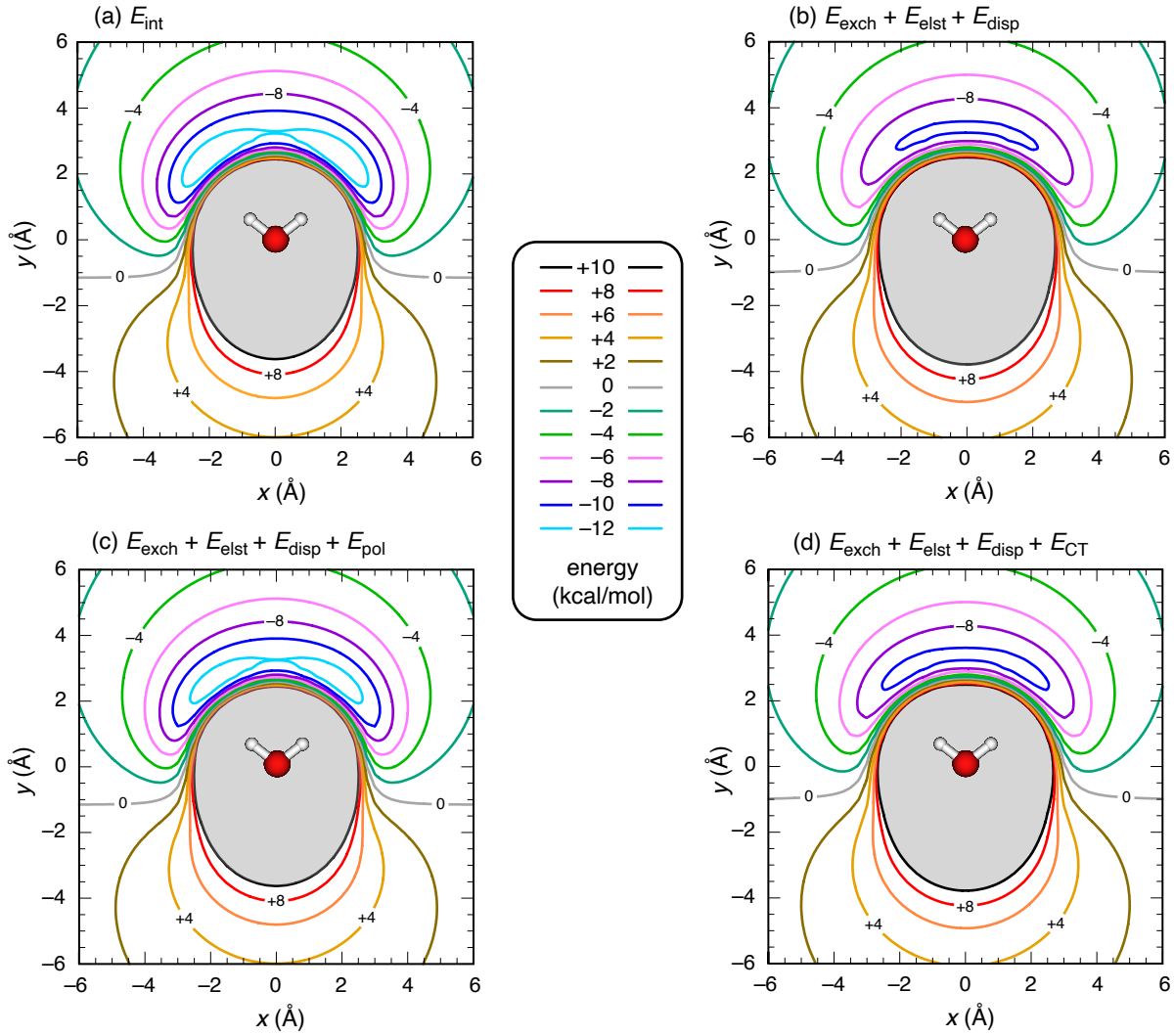

Figure S4: Contour plots of the chloride–water interaction potential and its sequential construction from SAPT energy components, scanning the position of Cl^- in the plane of a fixed-geometry H_2O molecule. Shown are (a) the full interaction potential, E_{int}; (b) $E_{int} - E_{ind} = E_{exch} + E_{elst} + E_{disp}$, where the entirety of the SAPT induction energy ($E_{ind} = E_{pol} + E_{CT}$) has been removed, and which (for a given Cl$\cdots$O distance) is rather flat for $|\theta_{ClOH}| \lesssim \theta(H_2O)/2$; (c) $E_{int} - E_{CT}$; and (d) $E_{int} - E_{pol}$. The potentials in (c) and in (d) each include one part of the SAPT induction energy (E_{pol} or E_{CT} but not both). The H_2O geometry is indicated (with oxygen at the coordinate origin) and corresponds to the isolated-monomer geometry optimized at the MP2/aug-cc-pVTZ level. Energy components were computed at the SAPT0 + δE_{HF}/jun-cc-pVDZ level on a grid of points extending to ±6.0 Å in both x and y, with $\Delta x = 0.25$ Å $= \Delta y$. Regions more repulsive than +10 kcal/mol are shaded in gray.

Table S1: Energies (in kcal/mol) for $X^-(H_2O)$.

X	Hydrogen-Bonded Minimum				C_{2v} Saddle Point				ΔE^a			
	CCSD(T)[b]		E_{int}(SAPT)		CCSD(T)[b]		E_{int}(SAPT)		CCSD(T)[b]		E_{int}(SAPT)	
	E_{bind}	E_{int}	SAPT0[c]	XSAPT +MBD[d]	E_{bind}	E_{int}	SAPT0[c]	XSAPT +MBD[d]	E_{bind}	E_{int}	SAPT0[c]	XSAPT +MBD[d]
F	−27.6	−32.9	−34.2	−31.4	−20.3	−23.8	−24.0	−22.9	7.3	9.1	10.2	8.5
Cl	−15.0	−15.7	−14.8	−17.6	−13.5	−14.8	−14.2	−16.0	1.5	0.9	0.6	1.6
Br	−14.0	−14.6	−12.6	−15.0	−12.8	−13.9	−12.5	−14.1	1.2	0.7	0.1	0.9
I	−11.9	−12.3	—	—	−11.3	−12.2	—	—	0.6	0.1	—	—

[a] $\Delta E = E(C_{2v}) - E(\text{H-Bond})$. [b] aug-cc-pVQZ(-PP) basis with a frozen core for F, Cl, and O, and an effective core potential for Br and I. [c] All-electron SAPT0 + δE_{HF}/jun-cc-pVDZ. [d] XSAPT+MBD+δE_{HF} [1]/def2-TZVPPD with CM5 charge embedding,[2] using the LRC-ωPBE functional (with ω_{GDD} tuning[3]) to describe the monomer wave functions.

References

[1] Carter-Fenk, K.; Lao, K. U.; Liu, K.-Y.; Herbert, J. M. Accurate and efficient *ab initio* calculations for supramolecular complexes: Symmetry-adapted perturbation theory with many-body dispersion. *J. Phys. Chem. Lett.* **2019,** *10,* 2706–2714.

[2] Liu, K.-Y.; Carter-Fenk, K.; Herbert, J. M. Self-consistent charge embedding at very low cost, with application to symmetry-adapted perturbation theory. *J. Chem. Phys.* **2019,** *151,* 031102:1–7.

[3] Lao, K. U.; Herbert, J. M. Atomic orbital implementation of extended symmetry-adapted perturbation theory (XSAPT) and benchmark calculations for large supramolecular complexes. *J. Chem. Theory Comput.* **2018,** *14,* 2955–2978.